JOURNAL OF CATALYSIS **171,** 374–382 (1997)
ARTICLE NO. CA971807

Preparation, Characterization, and Activity for *n*-Hexane Reactions of Alumina-Supported Rhodium–Copper Catalysts

A. Guerrero-Ruiz,* B. Bachiller-Baeza,† P. Ferreira-Aparicio,† and I. Rodríguez-Ramos†,[1]

*Departamento de Química Inorgánica, Facultad de Ciencias, UNED, 28040 Madrid, Spain; and †Instituto de Catálisis y Petroleoquímica, CSIC, Campus Cantoblanco, 28049 Madrid, Spain

Received February 14, 1997; revised May 2, 1997; accepted June 17, 1997

Alumina-supported rhodium–copper catalysts were prepared and characterized by chemisorption of hydrogen, temperature-programmed reduction, X-ray photoelectron spectroscopy, and infrared spectroscopy of adsorbed CO. It is shown that the alumina support interacts with rhodium as well as with copper. None of the bimetallic catalysts have a single phase, but are composed of segregated phases of rhodium and copper and alloyed clusters, the latter being formed at the lowest rhodium loading. The catalytic properties of the catalysts were studied by means of the *n*-hexane reaction. The turnover frequencies remained constant upon incorporation of copper into rhodium catalysts. However, the selectivity pattern changed; i.e., the isomerization reaction was enhanced at the expense of the hydrogenolysis reaction. The hydrogenolysis product distribution also shifted to a lower fragmentation factor. These results were explained by an ensemble effect in which the addition of copper isolates the rhodium in small clusters.

INTRODUCTION

Bimetallic catalysts have long been the focus of industrial and scientific interest. Most recent advances in heterogeneous catalysis have come from their wide spread use (for example, naphta reforming). Bimetallic catalysts often exhibit higher activity and/or selectivity or resistance to catalyst poisons, thus making them superior in many cases to the single component systems (1–5).

Bimetallic catalysts are defined as a mixture of two metals either in the form of an alloy or in the form of a cluster of the two metal atoms. Consequently, the structure of bimetallic catalysts is the most important factor in determining their performance. Even if we suppose a simple situation where the two metals form an alloy, this may be complicated by the movement of one of the metals to the surface, thus giving it a different composition to that of the bulk. The component with the lower heat of sublimation is often found at the surface (6) and, in the case of group VIII-group Ib combinations, this component is the group Ib metal. Moreover, theoretical calculations (7, 8) on bimetallic catalysts predict that a preferential localization of the more volatile component should occur at the sites of lower coordination. However, this topological segregation at kinks or steps still appears to be inferred from its theoretical plausibility (9). Up to now spectroscopic techniques such as EXAFS allow an estimate of the extent of surface enrichment but do not provide evidence of the surface topology.

On the other hand, the formation of bimetallic particles is also affected by the support, because the support may, apparently, affect the mobility of the precursors. The effects of MgO and SiO_2 over Ru−Au have been systematically compared (10, 11). On an SiO_2 support, the surface and bulk compositions of the bimetallic particles were similar. In contrast, MgO-supported Ru−Au particles show a surface enrichment in Ru instead of Au. This behavior has been explained by a strong interaction between MgO and the Au precursor, which prevented the migration of Au to the surface. Thus, the difficulty in obtaining accurate information about the surface topology complicates the elucidation of the mechanism to explain the catalytic effect of bimetallic catalysts.

Both a change in adsorption bond strength between chemisorbed adsorbates and surface-active metal atoms (ligand effect) and a dilution of the surface-active metal atoms to decrease the active ensemble size by the inactive metal (ensemble effect) are the controlling factors in determining the catalytic action of bimetallic catalysts. Thus, an investigation of catalytic reactions, that require a large number of neighboring surface atoms, can shed some light on the surface structure of the bimetallic catalysts. Conversion reactions of hydrocarbons are sensitive to the surface structure of the platinum metals (12–15). The catalytic properties of the $RhCu/SiO_2$ system in the conversion of a series of alkanes: *n*-hexane, 2-methylpentane, 2,2-dimethylbutane, 2,2,3,3-tetramethylbutane, methylcyclopentane were studied (16). The experimental results suggest that Cu occupies preferentially the site of low coordination, edges and corners, and Rh the sites of high coordination on dense planes. However, a detailed investigation of

[1] Corresponding author. E-mail: IRODRIGUEZ@ICP.CSIC.ES.

0021-9517/97 $25.00

the catalytic properties of the $RhCu/Al_2O_3$ system has not yet been reported. The aim of the present work is to study the surface properties of $RhCu/Al_2O_3$ catalysts of various compositions and their catalytic behavior in the *n*-hexane reaction.

EXPERIMENTAL

The catalysts were prepared by coimpregnation with aqueous solutions of the salts, according to the incipient wetness technique. The support used was γ-alumina Puralox from Condea ($S_{BET} = 175\ m^2 \cdot g^{-1}$). The salts were $RhCl_3 \cdot xH_2O$ (Aldrich Chemie) and $Cu(NO_3)_2 \cdot 3H_2O$ (Alfa). The total metal loading was maintained at around 5 wt%, and the Rh/Cu atomic ratio was adjusted to 0.05, 0.14, 0.23, and 0.43. After impregnation, the catalysts were dried overnight at room temperature and then calcined in air at 773 K for 3 h. The prepared catalysts and the chemical compositions, measured by atomic absorption, are listed in Table 1.

Hydrogen chemisorption measurements were performed in a Micromeritics 2700 Pulse Chemisorb apparatus. Samples of 0.4 g were first reduced in a $20\ cc \cdot min^{-1}$ hydrogen flow at 673 K for 2 h, cleaned under a flow of argon, and then cooled to room temperature, at which chemisorption measurements were made.

Temperature-programmed reduction (TPR) experiments were performed with aliquots of catalysts (300 mg) placed between two quartz wool plugs in a U-shaped quartz reactor. A high purity mixture of 6% hydrogen in helium was fed into the reactor. The temperature of the sample was increased from room temperature to 873 K at a rate of $5\ K \cdot min^{-1}$. The effluents of the reactor were monitored by a gas chromatograph (Varian 3400) provided with a thermal conductivity detector, an automatic sample injection, and a Porapak Q column. Individual analyses were perfomed at intervals of 2.5 min.

X-ray photoelectron spectra (XPS) were measured on samples reduced at 673 K for 2 h and exposed to air. The spectra were acquired with a Physical Electronics 5700 spectrometer equipped with a hemispherical multichannel Electronics 80-365B analyser. The pressure in the analysis chamber was kept below 10^{-9} Torr during acquisition. The excitation source was the Mg Kα line ($h\nu = 1253.6$ eV, 300 W). All binding energies were referenced to the adventitious C1s line at 284.8 eV.

The infrared spectra were recorded on a Nicolet 5 ZDX Fourier Transform IR spectrophotometer equipped with an MCT detector with a resolution of $4\ cm^{-1}$. Self-supporting wafers of the samples with weight-to-surface ratios of about $10\ mg \times cm^{-2}$ were placed in a vacuo cell assembled with greaseless stopcocks and KBr windows. Pretreatments were carried out with an *in-situ* furnace. The specimens were reduced in 70 Torr of H_2 at 373, 473, 573, and 673 K for 1 h and outgassed at 473 K for 1 h. After cooling to room temperature, the CO (60 Torr) was adsorbed and the IR recorded after removing the gas phase. For the sample reduced at 673 K, the CO desorption in vacuo was investigated by increasing the temperature at $5\ K \cdot min^{-1}$ in 50 K steps. The time in vacuo at each temperature was 10 min. The infrared spectra of the adsorbed species were obtained by subtracting the spectrum of the clean sample from the spectrum obtained after adsorption. All spectra were smoothed and the baseline corrected.

The *n*-hexane reaction was carried out in a fixed bed quartz reactor at atmospheric pressure (14). A catalyst charge between 12 and 13 mg was used to keep conversions below 15%. The *n*-hexane was fed into the reactor by bubbling a flow of hydrogen ($20\ cc \cdot min^{-1}$) through a saturator-condenser maintained at 293 K. The $H_2/n\text{-}C_6H_{14}$ molar ratio was 5.3. The catalysts were prereduced for 2 h at 673 K in a $20\ cc \cdot min^{-1}$ hydrogen flow. Then each catalyst was heated to the reaction temperature (750 K) at which the reaction mixture was fed. The effluents of the reactor were analysed by an on-line gas chromatograph (Varian 3400) provided with a thermal conductivity detector and a 30% DC-200 Chromosorb P-AW column.

Gases used for this study were He (99.9990% purity), Ar (99.998% purity), and H_2 (99.995% purity). Hydrogen was further purified in a deoxotrap and then passed through a molecular sieve, where trace quantities of water were removed from the hydrogen and helium flows.

TABLE 1

Main Characteristic and Chemisorption Data of the Catalysts

Sample	Metal loading		Chem.	XPS			H_2 uptake	
	%Rh	%Cu	Rh–Cu (atom%)	Rh–Cu (atom%)	Cu/Al	Rh/Al	(μmol/gcat)	H/Rh
Rh	1.25	—	100–0	100–0	—	0.18	23.2	0.38
Cu	—	4.84	0–100	—	—	—	—	—
0.05RhCu	0.45	4.6	5–95	4–96	0.08	0.003	8.6	0.39
0.14RhCu	0.95	4.2	12–88	—	—	—	14.9	0.32
0.23RhCu	1.40	3.8	19–81	11–89	0.10	0.01	24.8	0.36
0.43RhCu	2.05	3.0	30–70	—	—	—	14.0	0.14

RESULTS AND DISCUSSION

Table 1 summarizes the M/Al (M = Rh or Cu) ratios and metal atomic concentrations obtained by XPS and those derived from chemical composition. It can be seen that there is a strong resemblance between the bulk and XPS atomic concentration for the 0.05RhCu catalyst. However, for the 0.23RhCu catalyst, the XPS data show a slight enrichment in copper. This might indicate that rhodium atoms are uniformly distributed within the support pores, while copper is concentrated in the outer part of the pores. Comparison of the Rh/Al XPS ratio for 0.23RhCu with that of the monometallic rhodium catalyst reveals that the presence of copper alters the distribution of rhodium on the alumina, giving rise to a deeper penetration of rhodium atoms within the alumina pores. Therefore, the XPS technique provides valuable information on the location and distribution of the supported phase in the porous structure of the support.

Table 1 also gives the hydrogen uptake at room temperature on the alumina-supported Rh–Cu catalysts. Copper does not chemisorb H_2 at room temperature; therefore, H_2 chemisorption was used to determine the number of rhodium surface atoms. An adsorption stoichiometry of a hydrogen atom per surface rhodium atom was assumed. It was observed that, on the Rh–Cu catalysts, the H/Rh ratio remains more or less constant in the range of 5 to 19% atom Rh in the bulk. However, when the content increases to 30% atom Rh, the H/Rh decreases. Comparison of the monometallic Rh catalyst with the 0.23RhCu catalyst, with similar rhodium loading, shows that the H/Rh ratio does not decrease significantly upon Cu addition, as reported previously (16–18). However, it does not increase, although rhodium in the bimetallic catalyst is distributed more uniformly in the alumina pores, as shown by XPS.

To gain insight into the characterization of the catalysts, TPR experiments were performed. Figure 1 displays the TPR profiles for alumina-supported Rh, Cu, and Rh–Cu catalysts. The areas under the TPR curves were integrated for the different catalysts, giving amounts of hydrogen consumption which correspond in all cases to the complete reduction of Rh^{3+} and/or Cu^{2+} to Rh^0 and/or Cu^0. The TPR profile of the Cu catalyst shows a narrow peak at 470 K and a very broad peak at about 550 K with a long tail at the high temperature side. In agreement with results reported previously (19), the low temperature peak is assigned to the reduction of Cu^{2+} ions in highly dispersed copper oxide species (surface copper aluminate and small CuO entities interacting strongly with the alumina). The broad peak is attributed to the reduction in the bulk-like CuO phase. It has been observed previously (20, 21) that Cu^+ ions stabilize in the surface spinel layer, and their reduction proceeds at higher temperatures. Very recently, the state of the copper species in the Cu/Al_2O_3 catalyst was studied (22) by *in situ* X-ray absorption near the edge structure (XANES)

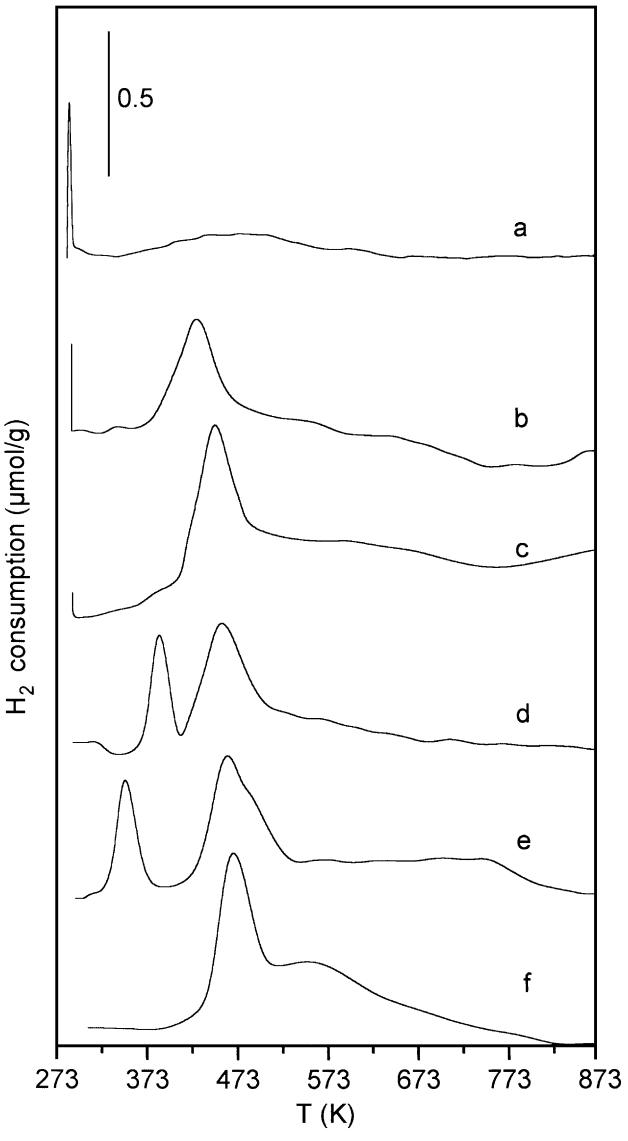

FIG. 1. TPR profiles of the different alumina-supported catalysts (a) Rh, (b) 0.43RhCu, (c) 0.23RhCu, (d) 0.14RhCu, (e) 0.05RhCu, (f) Cu.

during TPR in hydrogen. It was found that the Cu^{2+} ions in the surface copper aluminate reduce to Cu^+ ions at 473 K. The further reduction of Cu^+ ions in aluminate to Cu^0 occurs, together with that of the CuO phase at 550 K. The TPR profile (Fig. 1) of the alumina-supported rhodium catalyst shows a peak at room temperature and a broad feature centred at 473 K. The low temperature peak corresponds to the reduction of large particles of rhodium oxide. This is in agreement with the TPR studies made by Martin and Duprez (23) over Rh/alumina catalysts. They reported reduction temperatures in the range from room temperature to 363 K and found that the greater the rhodium particle size, the lower the maximum temperature reduction. The second peak in the TPR profile is the main contribution and

is assigned to the reduction of rhodium oxide strongly interacting with the alumina. This species has been reported to be created during calcination at temperatures above 773 K (24–26).

Comparison of the TPR profiles of the monometallic catalysts with those corresponding to the bimetallic RhCu catalysts show that rhodium slightly assists the reduction of copper. Thus, the main reduction peak of copper moves slightly to lower temperatures as the proportion of Rh increases in the bimetallic catalyst. The long tail at high temperature, attributed to Cu^+ in the aluminate and CuO phases, remains unchanged. As for the rhodium component, the low temperature reduction peak appears at room temperature when the rhodium loading is higher than 1 wt%. However, when the rhodium loading is lower than 1 wt% rhodium becomes more difficult to reduce, reducing in fact at about 350–390 K. The decreased reducibility of rhodium is thought to arise from an interaction of small amounts of rhodium with the copper oxide clusters (27, 28). In this case, the reduction of the rhodium, in close contact with various amounts of copper oxide, could lead to the formation of well-defined alloys. This is in agreement with observations made by Gentry and Hurst (27, 28) in their TPR studies of cupric oxide/transition metal samples. On the other hand, the rhodium oxide interacting with the alumina reduces in the same region as the CuO phase and Cu^+ ions in aluminate. As a consequence, it cannot be determined whether the reduction of this phase is altered by the presence of copper.

The TPR profiles for the alumina-supported Rh–Cu catalysts suggest, in principle, the presence of segregated phases, showing a rhodium (or rhodium-rich) phase and two phases of copper (copper aluminate and pure copper oxide). Similar findings were proposed for $Rh–Cu/SiO_2$ catalysts (16, 29). This observation was predicted by semiempirical rules developed by Burton *et al.* (7), stating that segregation occurs if the separation between liquid and solid in the phase diagram is large, as is the case for the Rh–Cu system (30).

To obtain further information on the composition and chemical properties of the catalyst's surface, the adsorption of CO was studied by infrared spectroscopy. The infrared spectra of CO adsorbed at room temperature on Rh/Al_2O_3 and Cu/Al_2O_3 catalysts reduced at successively increasing temperatures are shown in Figs. 2 and 3, respectively. CO adsorption on Rh/Al_2O_3 led to two bands at 2090

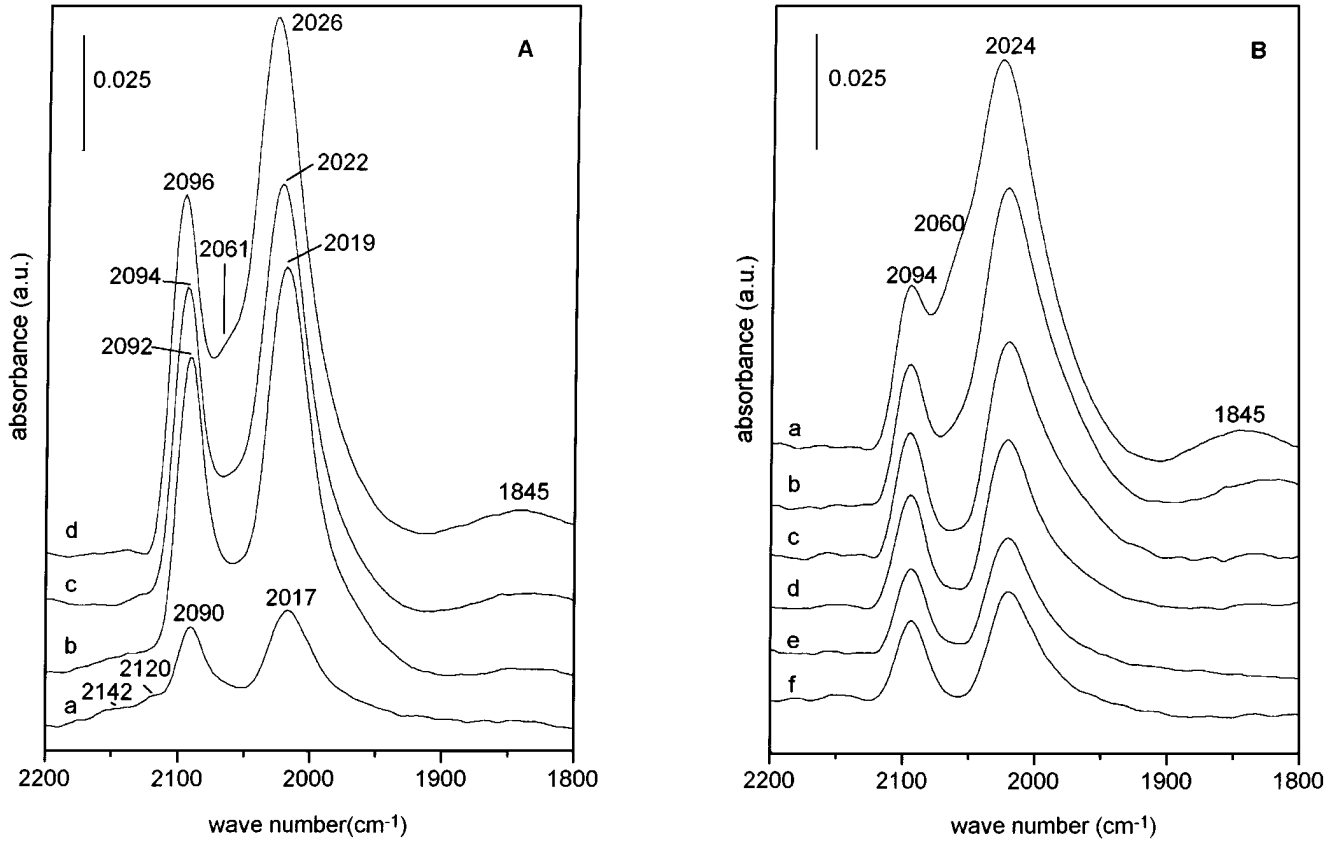

FIG. 2. Infrared spectra of CO adsorbed on the pure Rh catalyst: (A) reduced at (a) 373 K, (b) 473 K, (c) 573 K, (d) 673 K; (B) reduced at 673 K (a) complete CO chemisorption at 298 K, (b) after heating in vacuum at 373 K, (c) 423 K, (d) 473 K, (e) 523 K, (f) 573 K.

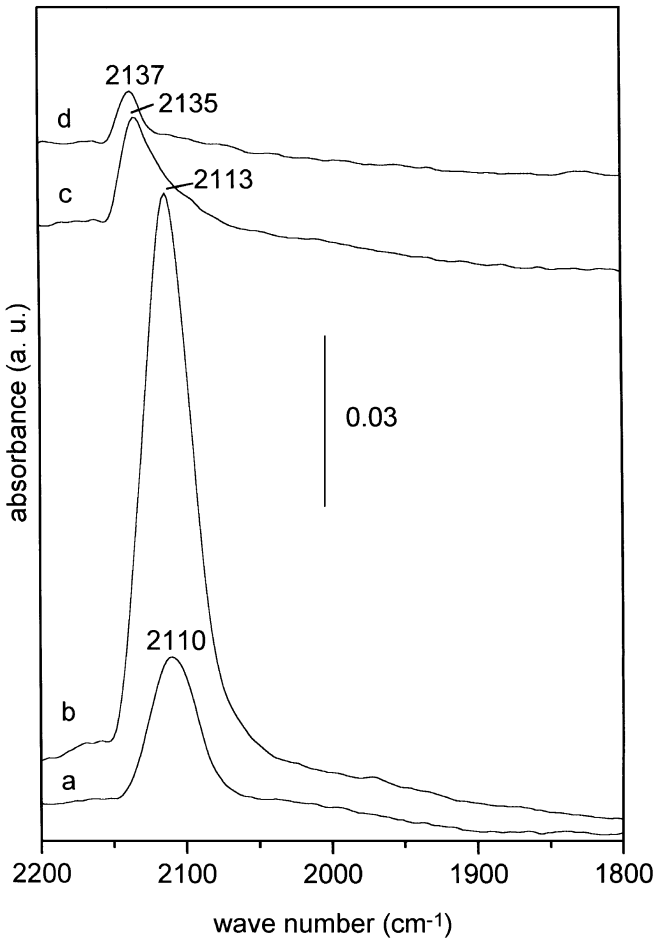

FIG. 3. Infrared spectra of CO adsorbed on the pure Cu catalyst reduced at (a) 373 K, (b) 473 K, (c) 573 K, (d) 673 K.

and 2017 cm^{-1} (Fig. 2A.) whose intensity was greatest following reduction at 473 K. A shoulder at 2061 cm^{-1} and a weak and broad band at 1845 cm^{-1} also developed at higher reduction temperatures. In accordance with literature data (31), CO frequencies at 2090 and 2017 cm^{-1} are assigned to the symmetrical and asymmetrical stretching vibration of the dicarbonyl complex on isolated Rh^+ ions (32, 33). For the existence of Rh^+ the CO-induced disruption of small Rh crystallites to isolated Rh atoms, which are readily oxidized to Rh^+ with the OH groups of the support, has been proposed (32–35). Bands at 2060 and 1845 cm^{-1} are ascribed to linear- and bridge-bonded CO, respectively, on crystalline Rh^0. In agreement with TPR study (Fig. 1), the infrared results show that the Rh/Al_2O_3 catalyst is still partially oxidized after reduction at 373 K. In addition to the low intensity of the bands of dicarbonyl species, weak bands appear above 2100 cm^{-1}, i.e., in the range of CO adsorbed on oxidized rhodiums; bands at 2120 and 2142 cm^{-1} are assigned to Rh^{2+} and Rh^{3+}, respectively (36). Since dicarbonyls correspond to the dispersed phase and linear- and bridge-bonded CO to crystalline rhodium, a growing number of larger clusters can be inferred when the reduction temperature is increased. The shift to higher wave numbers for the two dicarbonyl bands can also be attributed to increased sintering at higher reduction temperatures (36). This is because of the higher local density of adsorbed CO molecules on larger clusters which results in stronger dipolar coupling.

The stability of the CO species adsorbed at room temperature on the Rh/Al_2O_3 catalyst reduced at 673 K was studied by thermal desorption under vacuum. The spectra obtained as temperatures are increased step-wise and are shown in Fig. 2B. A loss in band intensities of the linear- and bridge-bonded CO on Rh^0 was noted immediately at 373 K. Above 373 K the decline in dicarbonyl bands became progressively slower. While the linear- and bridge-bonded CO species on Rh^0 disappeared at 423 K, the dicarbonyl species were still apparent at 573 K. These observations confirm those of previous workers (37) that CO species adsorbed on Rh^0 (linear- and bridge-bonded) are more weakly held than dicarbonyl species on Rh^+.

Upon exposure to CO at room temperature and outgassing, the Cu/Al_2O_3 catalyst reduced at 373 K displays a weak band at 2110 cm^{-1} (Fig. 3). After the sample was reduced to 473 K, a strong band was found at 2113 cm^{-1}. Bands in the spectral region of 2080–2110 cm^{-1} have been attributed previously to CO adsorbed on large particles of metallic copper (38) as well as to Cu^+–CO complexes in three-dimensional CuO clusters (39). According to Davydov *et al.* (38), bands in the spectral region of 2110–2140 cm^{-1} correspond to CO adsorbed on Cu^+ ions. The TPR results indicate that following reduction at 473 K, copper in the spinel phase is reduced partially to Cu^+, and the further reduction of this and CuO phase proceeds at higher temperatures. Therefore, the band at 2110–2113 cm^{-1} can be assigned to CO adsorbed on Cu^+ sites in the copper aluminate phase. If the temperature of reduction is increased to 573 K and subsequently to 673 K, the band intensity of CO is strongly decreased, with the observation of small components at 2117 and 2135 cm^{-1}. These spectral features are a result of the further reduction of Cu^+ ions in aluminate, followed by subsequent sintering, which leads to some bands at higher frequency corresponding to CO adsorbed on Cu^+.

For the alumina-supported Rh–Cu catalysts reduced at subsequently increasing temperatures, the room temperature infrared spectra of adsorbed CO are shown in Figs. 4 and 5. It is observed that the spectra are affected by the Rh–Cu proportion. The 0.23Rh–Cu (Fig. 4A) show spectra at the successive reduction temperatures that are essentially the same as those of the pure Rh catalyst, i.e. two strong dicarbonyl bands at 2024 and 2096 cm^{-1} on Rh^+ and, following reduction at 573 K and above, a shoulder at 2059 cm^{-1} stemming from linear-bonded CO on Rh^0.

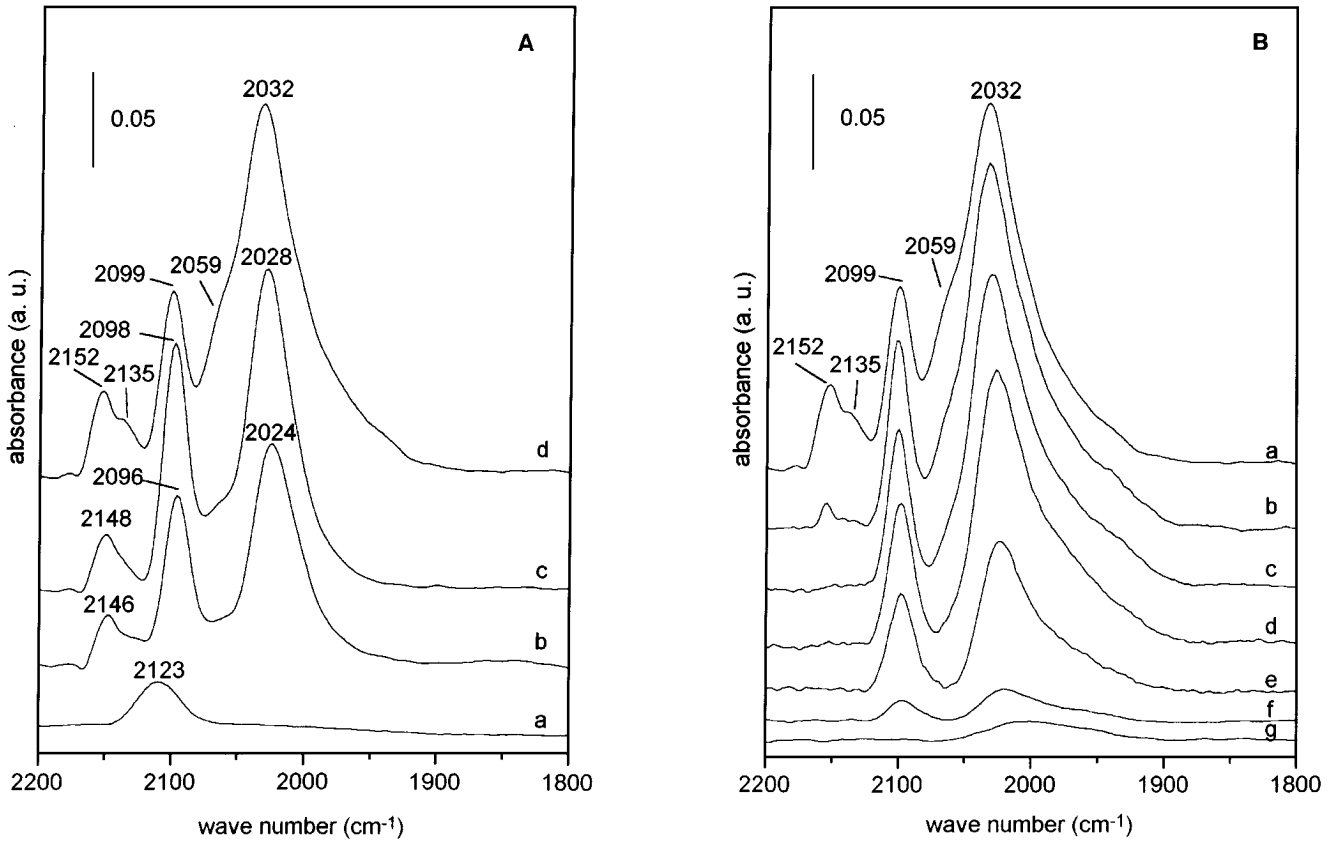

FIG. 4. Infrared spectra of CO adsorbed on the 0.23RhCu catalyst: (A) reduced at (a) 373 K, (b) 473 K, (c) 573 K, (d) 673 K; (B) reduced at 673 K (a) complete CO chemisorption at 298 K, (b) after heating in vacuum at 373 K, (c) 423 K, (d) 473 K, (e) 523 K, (f) 573 K, (g) 623 K.

However, the comparison of these spectra (Fig. 4A) with those of the monometallic copper catalyst (Fig. 3) confirms the findings of the TPR experiments (Fig. 1) that the presence of Rh in loadings higher than 1 wt% assists the reduction of copper. The 0.23RhCu reduced at 373 K (Fig. 4) displays a broad band with a maximum at 2123 cm^{-1} which suggests that CO is adsorbed over a wide distribution of Cu^+ sites, probably located in a $CuAl_2O_4$ phase and in small CuO clusters anchored to the alumina surface. Upon treatment in hydrogen at 473 K the Cu^+ in the spinel phase is almost completely reduced and also sintered. Only small contributions at 2146 and 2135 cm^{-1}, due to CO adsorbed on Cu^+ in the aluminate phase, are observed. The spectral feature of copper in 0.23RhCu reduced at 373 and 473 K resembles that of the pure copper sample reduced at 473 and 573 K, respectively.

A different picture is found for the bimetallic Rh–Cu catalyst with 5% atom Rh (Fig. 5A). The spectra of adsorbed CO are the sum of those obtained for the monometallic rhodium (Fig. 2A) and copper (Fig. 3) samples after similar reduction treatments. In addition, a new band at 1999 cm^{-1} develops as a shoulder at 473 K and becomes clearly resolved in the 573 K reduced 0.05RhCu sample. This 1999 cm^{-1} band could be attributed to linearly bound CO on Rh^0 in a mixed Rh–Cu phase. It is known that frequency changes in the IR absorption bands can occur as a result of alloying (3). For alloys which are formed with a small or moderate exothermic effect, these shifts are caused largely by changes in dipole–dipole coupling effects (40). The dilution of the rhodium atoms by the copper would lead to an increase in the average distance between adsorbed CO molecules which would decrease dipole–dipole coupling and lower the observed vibration frequency. The intensity of the 1999 cm^{-1} band decreases for the 0.5RhCu sample reduced at 673 K and, simultaneously, a shoulder grows at 2059 cm^{-1} due to linear-bonded CO on crystalline Rh^0. This fact reveals that, at higher temperatures of reduction, above 573 K, the Rh–Cu alloy partially segregates into crystalline Rh^0 and Cu^0 phases.

The low frequency band at 1845 cm^{-1}, due to bridge-bonded CO on Rh^0, was suppressed for the Rh–Cu catalysts, both with high and low loadings of Rh (Figs. 4A and 5A), indicating that the rhodium surface atoms on bimetallic catalysts are not in the form of ensembles that chemisorb bridged CO. Similar results were found for Cu–Rh/SiO_2 catalysts (41).

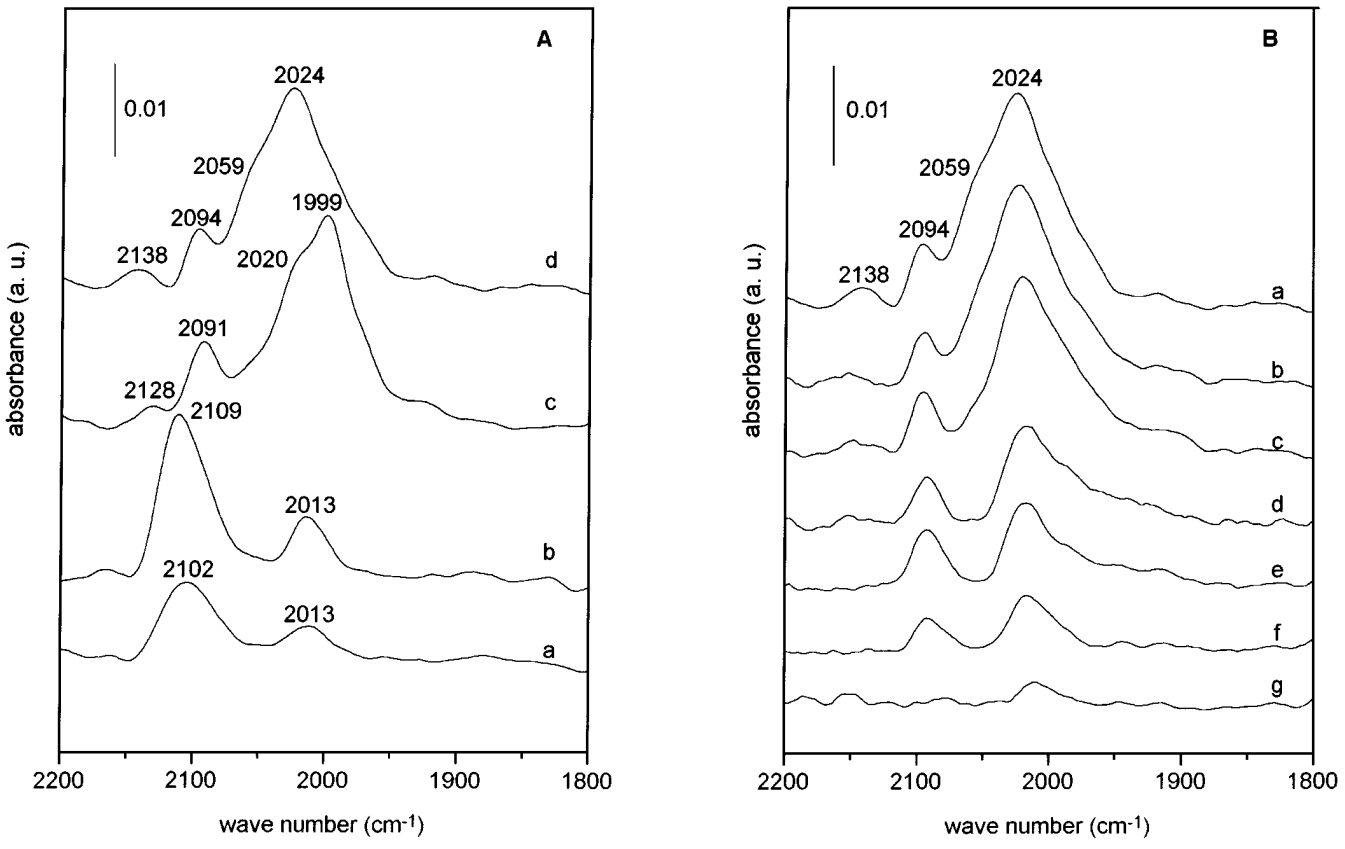

FIG. 5. Infrared spectra of CO adsorbed on the 0.05RhCu catalyst: (A) reduced at (a) 373 K, (b) 473 K, (c) 573 K, (d) 673 K; (B) reduced at 673 K (a) complete CO chemisorption at 298 K, (b) after heating in vacuum at 373 K, (c) 423 K, (d) 473 K, (e) 523 K, (f) 573 K, (g) 623 K.

On the other hand, the stability of the CO species adsorbed at room temperature on the RhCu catalysts reduced at 673 K was studied by thermal desorption in vacuum. The spectra obtained are shown in Figs. 4B and 5B. CO species adsorbed on copper are less stable than those on rhodium, since these disappear at 423 K, while CO species on rhodium are still found at 623 K.

Finally, we conducted a test reaction, the conversion of *n*-hexane, to learn about the coordination of the surface rhodium atoms. For all catalysts, catalytic activities and selectivities were compared at 750 K. The results obtained are reported in Table 2. The following parameters were evaluated: conversion of *n*-hexane $= (\Sigma i/6C_i/(C_6 + \Sigma i/6C_i))100$, selectivity in i compound $= (iC_i/\Sigma iC_i)100$, where C_i is the molar concentration of product i and C_6 is the molar concentration of *n*-hexane. Activities are expressed as turnover frequency (TOF) or number of molecules of *n*-hexane converted per surface rhodium atom. Since the activity of rhodium is two orders of magnitude larger than that of copper, the specific activity of the samples may be ascribed to the surface rhodium atoms. In addition to the selectivity pattern in *n*-hexane conversion (hydrogenolysis, isomerization, and dehydrogenation reactions), the distribution of various fragments in the hydrogenolysis reaction may offer a host of information about possible active sites. Thus, the distribution of hydrogenolysis products and the fragmentation factor are given in Table 3. The latter characterizes the depth of hydrogenolysis and represents the number of hydrocarbon fragments per decomposed molecule (42), $\xi = \Sigma C_i/(\Sigma i/6C_i)$. A value of 2 reflects the splitting of one single bond, whereas $\xi > 2$ shows the occurrence of multiple fragmentations (methanisation).

TABLE 2

Catalytic Properties of the Different Catalysts for the Conversion of *n*-Hexane[a]

Sample	Conv. (%)	TOF (s^{-1})	Product selectivity (%)		
			C_1–C_5	i-C_6	bz
Rh	11.8	0.28	78	9	12
Cu	2.8	1.30[b]	26	74	0
0.05RhCu	5.8	0.35	68	20	12
0.14RhCu	12.6	0.37	78	11	11
0.23RhCu	17.5	0.35	82	6	13
0.43RhCu	10.2	0.71	78	8	14

[a] Reaction temperature, 750 K; H_2/*n*-$C_6H_{14} = 5.3:1$; time on-stream, 105 min.

[b] Catalytic activity is expressed as μmol/gcat · s.

TABLE 3

Distribution of Hydrogenolysis Products[a]

Sample	Conv. (%)	Fragment distribution (%)					
		C_1	C_2	C_3	C_4	C_5	ξ
Rh	11.8	91	5	3	1	1	5.1
Cu	2.8	10	24	33	30	4	2.1
0.05RhCu	5.8	77	9	5	5	4	4.0
0.14RhCu	12.6	83	7	4	3	2	4.5
0.23RhCu	17.5	86	7	3	2	2	4.7
0.43RhCu	10.2	84	7	4	3	2	4.5

[a] Reaction temperature, 750 K; $H_2/n\text{-}C_6H_{14} = 5.3:1$; time on-stream, 105 min.

After a slight decrease in initial activity (10–15%), no significant deactivation occurred during the course of the reaction. The activities of catalysts after 105 min on-stream are listed in Table 2. It is shown that the turnover frequencies for the *n*-hexane conversion were more or less constant upon incorporation of the inactive metallic element. The *n*-hexane conversion on Rh/Al_2O_3 can proceed by several routes and is not very sensitive to the structure (43, 44). On the basis of the ensemble theory (3), a small effect on turnover frequency is expected when the rhodium surface is diluted into small ensembles as copper is added.

With respect to the selectivity pattern for the *n*-hexane conversion, this remains approximately the same when the Rh/Cu atomic ratio in the bimetallic catalysts is 0.14 or higher. In contrast, the 0.05RhCu catalyst shows clear changes in the selectivity pattern. Thus, the selectivity for the isomerization reaction increases at the expense of the hydrogenolysis reaction, while the dehydrocyclation remains unchanged. Previous work with silica-supported Rh–Cu catalysts suggested that enhanced selectivities for isomerization of alkanes may follow the incorporation of Cu into Rh (16, 18, 45). On the other hand, the product distribution of the hydrogenolysis reaction changes with the introduction of copper, i.e. a fragmentation factor decrease.

The changes in the selectivity pattern of *n*-hexane conversion and hydrogenolysis product distribution parallel those reported previously on the influence of the rhodium particle size (43). The selectivity patterns shifted in the direction of small rhodium particles. To describe the catalytic properties of supported Rh catalysts (43) in the conversion of alkanes, two types of intermediates have been postulated: metallocarbenes or metallocycles which prevail for high coordinations of Rh surface atoms and which appear to be highly sensitive to the metallic dispersion, and π-adsorbed species which can occur with similar probabilities whatever the rhodium particle size. The former are the main species for the hydrogenolysis reaction (12). The changes in selectivity at the 0.05RhCu catalyst support the idea that Cu and Rh form true bimetallic particles, as above shown by IR of CO adsorbed on this catalyst. These results also indicate that copper is randomly distributed at the surface of the bimetallic particles, which isolates the rhodium in ensembles of small size. Thus, the *n*-hexane hydrogenolysis, requiring a carbene intermediate formed at high coordination sites (dense planes), is affected by alloying. In contrast, the coexistence of the two classes of intermediates explains the very low sensitivity to alloy of turnover frequency for *n*-hexane conversion.

This explanation agrees with a previous work on Rh–Cu silica-supported catalysts (16) in which the conclusion was reached that, at low copper loading ($Rh/Cu \geq 1$), copper tends to locate preferentially at corner and edge sites, and Rh forms islands large enough to behave like big rhodium clusters. With additional copper ($Rh/Cu = 0.33$), the surface concentration of copper becomes large enough to decrease the size of the rhodium islands and to isolate the rhodium atoms, reproducing the behaviour of very small Rh particles. However, in our system the Rh–Cu alloy is formed for a bulk formulation of Rh : Cu 5 : 95 atom% while this was 25 : 75 on silica (16). The different behaviour of the rhodium–copper system may be due to the distinct support used (alumina vs silica). Thus, the alumina interacts both with rhodium whose reducibility is decreased as shown by TPR (Fig. 1) and with copper, forming an aluminate. As a result, the rhodium–copper interaction is also different. Moreover, as described above by IR of adsorbed CO, our catalyst is not a pure phase but is composed of segregated rhodium and copper phases and the Rh–Cu alloy.

CONCLUSIONS

The characterization by TPR in hydrogen and by infrared of adsorbed CO and the study of the *n*-hexane reaction as a probe of surface properties provided information about alumina-supported Rh–Cu catalysts. Our conclusions are the following:

—The alumina support interacts both with rhodium, whose reducibility is reduced at lower loadings, and with copper giving an aluminate. These features condition the rhodium–copper aggregates when these are formed.

—The bimetallic Rh–Cu catalysts do not form a single alloyed phase. They are constituted by segregated phases of Rh and Cu as well as by a Rh–Cu alloy (in the 0.05 catalyst).

—Rh and Cu are distributed randomly at the surface of the mixed Rh–Cu ensembles. Their catalytic properties parallel those of very small clusters of rhodium. The effect of alloying is explained by the ensemble model in which the number of contiguous Rh atoms is decreased by dilution with copper atoms.

In summary, the conjunction of these different techniques is very useful for studying complex systems such as the supported bimetallic catalysts.

ACKNOWLEDGMENTS

This work was partially supported by CICYT, Spain (Project No. MAT96-0859-CO2-O2) and by DGICYT, Spain (Project No. PB94-0077-CO2-O2). Thanks are due to Dr. E. Rodríguez-Castellón of the University of Malaga for the XPS measurements.

REFERENCES

1. Campbell, C. T., *Annu. Rev. Phys. Chem*. **41**, 775 (1990).
2. Guczi, L., and Sárkány, A., *in* "Specialist Periodical Report, Catalysis" (J. J. Spivey and S. K. Agarwal, Eds.), Vol. 11, p. 318, Royal Society of Chemistry, London, 1994.
3. Ponec, V., *Adv. Catal.* **32**, 149 (1983).
4. Sinfelt, J. H., *Acc. Chem. Res.* **10**, 15 (1977).
5. Clarke, J. K. A., *Chem. Rev.* **775**, 291 (1975).
6. Sachtler, W. M. H., and van Santen, R. A., *Adv. Catal.* **26**, 69 (1977).
7. Burton, J. J., Hyman, E., and Fedak, D. G., *J. Catal.* **37**, 106 (1975).
8. Strohl, J. K., and King, T. S., *J. Catal.* **116**, 540 (1989).
9. Clarke, J. K. A., and Creaner, A. C. M., *Ind. Eng. Chem. Prod. Res. Dev.* **20**, 574 (1981).
10. Galvagno, S., Schwank, J., Parravano, G., Garbassi, F., Marzi, A., and Tanszik, G. R., *J. Catal.* **69**, 283 (1981).
11. Galvagno, S., Schwank, J., and Parravano, G., *J. Catal.* **61**, 223 (1980).
12. Gault, F. G., *Adv. Catal.* **30**, 1 (1981).
13. Maire, G. L. C., and Garin, F. G., *in* "Catalysis: Science and Technology" (J. R. Anderson and M. Boudart, Eds.), Vol. 6, p. 161. Springer-Verlag, Berlin, 1984.
14. Rodríguez-Ramos, I., and Guerrero-Ruiz, A., *Appl. Catal. A: General* **119**, 271 (1994).
15. Rodríguez-Reinoso, F., Rodríguez-Ramos, I., Moreno-Castilla, C., Guerrero-Ruiz, A., and López-Gonzalez, J. D., *J. Catal.* **107**, 1 (1987).
16. Coq, B., Dutartre, R., Figueras, F., and Rouco, A., *J. Phys. Chem*. **93**, 4904 (1989).
17. Meitzner, G., Via, G. H., Lyttle, F. W., and Sinfelt, J. H., *J. Chem. Phys.* **78**, 883 (1983).
18. Clarke, J. K. A., Manniger, I., and Baird, T., *J. Catal.* **54**, 230 (1978).
19. Dow, W.-P., Wang, Y.-P., and Huang, T.-J., *J. Catal.* **160**, 155 (1996).
20. Marques, E. C., Friedman, M. R., and Dahm, D. J., *Appl. Catal.* **19**, 387 (1985).
21. Sepúlveda, A., Marquez, C., Rodríguez-Ramos, I. A., Guerrero-Ruiz, A., and Fierro, J. L. G., *Surf. Interface Anal.* **20**, 1067 (1993).
22. Ferreira-Aparicio, P., Fernandez-Garcia, M., Rodríguez-Ramos, I., and Guerrero-Ruiz, A., unpublished.
23. Martin, D., and Duprez, D., *Appl. Catal.* **131**, 297 (1995).
24. Yao, H. C., Japan, S., and Shelef, M., *J. Catal.* **50**, 407 (1977).
25. Beck, D. D., Capehart, T. W., Wong, C., and Belton, D. N., *J. Catal.* **144**, 311 (1993).
26. Burch, R., Loader, P. K., and Cruise, N. A., *Appl. Catal. A: General* **147**, 375 (1996).
27. Gentry, S. J., Hurst, N. W., and Jones, A., *J. Chem. Soc. Faraday I* **77**, 603 (1981).
28. Hurst, N. W., Gentry, S. J., Jones, A., and MacNicol, B. D., *Catal. Rev.-Sci. Eng.* **24**, 233 (1982).
29. Foord, J. S., and Jones, P. D., *Surf. Sci.* **152**, 487 (1985).
30. Taylor, J. R., *Platinum Met. Rev.* **29**, 74 (1985).
31. Yang, A. C., and Garland, C. W., *J. Phys. Chem*. **61**, 1504 (1957).
32. Van't Blik, H. F. J., Van Zon, J. B. A. D., Huizinga, T., Vis, J. C., Koningsberger, D. C., and Prins, R., *J. Phys. Chem*. **87**, 2264 (1983).
33. Solymosi, F., and Pásztor, M., *J. Phys. Chem*. **89**, 4789 (1985).
34. Basu, P., Panayotov, D., and Yates, J. T., Jr., *J. Phys. Chem*. **91**, 3133 (1987).
35. Wong, T. T. T., Stakheev, A. Yu, and Sachtler, W. M. H., *J. Phys. Chem*. **96**, 7733 (1992).
36. Rice, C. A., Worley, S. D., Curtis, C. W., Guin, J. A., and Tarrer, A. R., *J. Chem. Phys.* **74**, 6487 (1981).
37. Yates, D. J. C., Murrell, L. L., and Prestridge, E. B., *J. Catal.* **57**, 41 (1979).
38. Lokhov, Yu A., and Davydov, A. A., *Kinet. Catal.* **20**, 1498 (1979).
39. Tikhov, S. F., Sadykov, V. A., Kryukova, G. N., Paukshtis, E. A., Popovskii, V. V., Starostina, T. G., Kharlamov, G. V., Anufrienko, V. F., Poluboyarov, V. F., Razodobarov, V. A., Bulgakov, N. N., and Kalikin, A. V., *J. Catal.* **134**, 506 (1992).
40. Toolenaar, F. J. C. M., Stoop, F., and Ponec, V., *J. Catal.* **82**, 1 (1983).
41. Krishnamurthy, R., Chuang, S. S. C., and Ghosal, K., *Appl. Catal. A: General* **114**, 109 (1994).
42. Paal, Z., and Tetenyi, P., *Nature* **267**, 234 (1977).
43. Coq, B., and Figueras, F. J., *Mol. Catal.* **40**, 93 (1987).
44. Coq, B., Dutartre, R., Figueras, F., and Tazi, T., *J. Catal.* **122**, 438 (1990).
45. Clarke, J. K. A., Rooney, K. M. G., and Baird, T., *J. Catal.* **111**, 374 (1988).